Azide click chemistry on magnetotactic bacteria: A versatile technique to attach a cargo

Paul Eduardo David Soto Rodriguez, Mila Sirinelli-Kojadinovic, Maximilien Rouzaud, Damien Faivre

▶ **To cite this version:**

Paul Eduardo David Soto Rodriguez, Mila Sirinelli-Kojadinovic, Maximilien Rouzaud, Damien Faivre. Azide click chemistry on magnetotactic bacteria: A versatile technique to attach a cargo. Materials Today Bio, 2023, 19, pp.100587. 10.1016/j.mtbio.2023.100587 . cea-04448209

HAL Id: cea-04448209
https://cea.hal.science/cea-04448209

Submitted on 9 Feb 2024

HAL is a multi-disciplinary open access archive for the deposit and dissemination of scientific research documents, whether they are published or not. The documents may come from teaching and research institutions in France or abroad, or from public or private research centers.

L'archive ouverte pluridisciplinaire **HAL**, est destinée au dépôt et à la diffusion de documents scientifiques de niveau recherche, publiés ou non, émanant des établissements d'enseignement et de recherche français ou étrangers, des laboratoires publics ou privés.

Title:

Azide click chemistry on magnetotactic bacteria: a versatile technique to attach a cargo

Authors:

Paul Eduardo David Soto Rodriguez[1], Mila Sirinelli-Kojadinovic[1], Maximilien Rouzaud[1] and Damien Faivre[1*]

[1] Aix Marseille University, CEA, CNRS, BIAM, 13108 Saint Paul-Lez-Durance, France

*Corresponding author

Email: Damien.FAIVRE@cea.fr

ABSTRACT:

Adding biomolecules to living organisms and cells is the basis for creating living materials or biohybrids for robotic systems. Bioorthogonal chemistry allows covalently modifying biomolecules with functional groups not natively present under biological conditions and is therefore applicable to microorganisms and cells. Click chemistry is a biorthogonal chemistry approach that allows the study and manipulation of living entities. Incorporating the bioorthogonal click-chemistry handle, azide groups, into living microorganisms has been achieved by metabolic labeling, i.e., by culturing cells or organisms in a modified culture media having a specific natural molecular building block (e.g., amino acid, nucleotide, carbohydrate) modified with a tagged chemical analog. Here we explore the effect of the azide group incorporation into the magnetotactic bacteria *Magnetospirillum gryphiswaldense* (MSR-1) by adding a modified amino acid, 3-Azido-D-Alanine, during their cultivation. We show the existence of a concentration limit to effectively incorporate the azide group while maintaining the magnetic properties of the cells. We explore the use of this modification to explore the combination with versatile single-cell tagging methods.

Keywords: (max6)

Click chemistry, magnetotactic bacteria, single-cell tagging

Introduction

Theranostics is one of the main application field of nano and micro-robotics [1]. Many designs developed for theranostics are based on mimicking microorganisms, particularly introducing motility and sensing functionalities [2]. Magnetic properties often provide or at least improve theranostic applications. Therefore, the attention on magnetic nanoparticles is rising in this area [3]. Another rising research field is the so-called bacteria bots, which studies the direct modification of bacterial surfaces to attach a cargo that can be used for detection and treatment of a given illness [4]. Different bacterial strains and cargo designs have been proposed [5–8]. The primary desired characteristics are that bacteria should allow easy attachment of biomolecules, be able to control and provide easy characterization remotely. Many bacteria have been genetically engineered or chemically modified to fulfill these properties, including nanoliposomes attachment through amine

coupling by activation of carboxylic acids with EDC/NHS chemistry [9], by NHS-ester amine coupling [10] or biotin-streptavidin reactions [11].

Magnetotactic bacteria (MTB) mineralize and organize intracellularly magnetic particles called magnetosomes. The latter allow them to swim along the geomagnetic field lines [12] and therefore enable magnetic control of MTB motility by external magnetic fields. In addition, MTB use a magnetically-biased aerotaxis that allows them to find their preferred living conditions [13]. This particular behavior has been used to develop active systems envisioned to deliver drugs to cancer cells [9,14]. Moreover, the magnetic properties of magnetosomes are used as a contrast agent in biomedical imaging applications. For example, for magnetic resonance imaging (MRI) when isolated [15], or as tracer particles in magnetic particle imaging (MPI) isolated [16] or even within the cell [17].

Click chemistry, topic for which the 2022 Nobel prize awards were given [18], refers to a set of fast reactions, easy to use, simple to purify, versatile, regiospecific, and with high product yields [18]. Click chemistry permits different biomolecules' easy and fast attachment to particles. The group of reactions mainly used is the Huisgen 1,3-dipolar cycloaddition of azides and terminal alkynes. To date, it has not been hardly exploited for its use in magneotactic bacteria. Indeed, the application of alkyne-azide click chemistry is not straightforward as the needed functional group azide is not naturally present in bacteria. Moreover, as shown in scheme 1 A, the conventional azide-alkyne binding is done with the help of copper(I) as a catalyst [19], which, in general, is harmful to bacteria at the concentration used [20]. However, there are methods to overcome these drawback. For example, azide groups can be incorporated into living animals by genetic engineering [21,22] or metabolic labeling and can therefore enable copper-free click chemistry to label biomolecules in mice [23]. In addition, copper-free strain-promoted azide-alkyne cycloaddition has already been developed and used as an alternative in living cells and was recently awarded with a Nobel prize 2022. For this method, a strained molecule (Dibenzocyclooctyne, DBCO) is used that can react with the azide without the need of the copper catalyst as show in Scheme 1B.

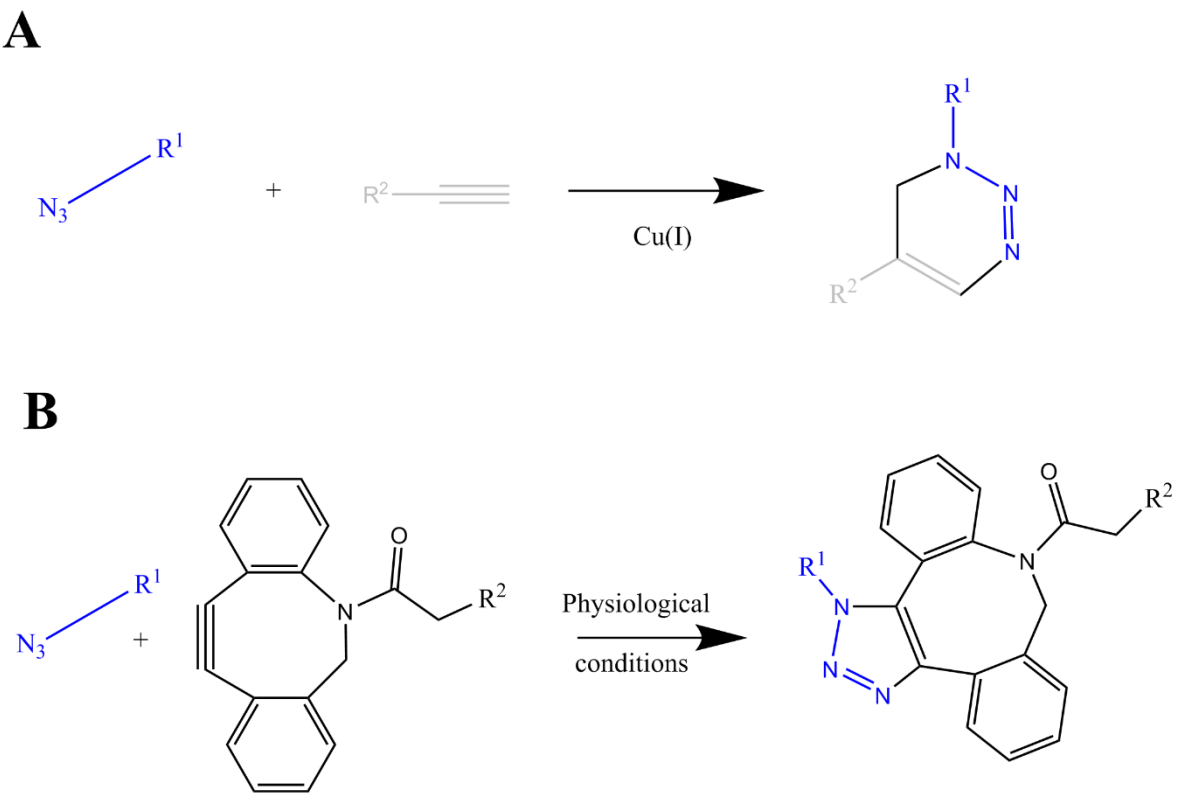

Scheme 1: Click chemistry. A) Copper(I)-catalyzed azide alkyne cycloaddition (CuAAC) mechanism. B) Copper free click chemistry with the strained Dibenzo cyclooctene (DBCO) molecule.

In the present work, we describe azide group incorporation by bacteria. This will pave the way for future click chemistry on bacterial surface, providing the necessary engineering tools to modify bacteria as needed with the reported advantage of MTB in terms of control and theranostics.

More precisely, we propose to couple MTB and copper-free strain-promoted azide-alkyne cycloaddition to join the advantages of these two separate entities. We thus feed MTB with a modified amino acid, 3-Azido-D-alanine, to enable click chemistry on their surface. The unnatural D-amino acids are incorporated into cell walls; the bioorthogonal (azide) group is cut and integrated into the surface [24]. We investigate bacterial physiological properties to determine how the incorporation of the modified amino acid impacts (cell growth, biomineralization capabilities and hence magnetic properties). We show that amino acid concentration must be controlled to avoid stressing bacteria. Finally, we show successful click chemistry by adding different fluorescent chemical compounds but also 10 µm-beads as cargos. These results will enable the facile chemical engineering of MTB for a given application.

Materials and methods

Materials

DBCO-PEG4-FLUOR 545; DBCO-Cy5; DBCO-dPEG ®12-carboxyfluorescein were purchased from ***Sigma Aldrich***, while the 3-Azido-D-Alanine Hydrochloride was purchased from ***BASECLICK***. Micromer®-DBCO 10 µm was purchased from ***micromod Partikeltechnologie GmbH***.

Methods

Bacterial cultivation and incorporation of the modified amino acid

Magnetospirillum gryphiswaldense (MSR-1) cells were grown at 28°C under microoxic conditions) in Hungate tubes containing 12 mL of modified Flask Standard Medium (FSM) containing 50 µM ferric iron citrate [25]. Bacterial cultures were started at low cell density, i.e., at OD (600 nm) ≅ 0.009 to 0.02, from pre-cultures in mid-stationary phase and were grown for three days. To effectively incorporate the amino acid and use the cells for further modification, the modified amino acid was added directly after bacterial inoculation. Three concentrations of 3-Azido-D-alanine were tested: 0.009 mM, 1.080 mM, and 1.800 mM .

Methods used to assert the effect of azide incorporation on the MTB magnetic properties

A customized magnetic microscope was used [26]. Briefly, the microscope has a triaxial Helmholtz coil set, a controller (C-SpinCoil-XYZ, Micro Magnetics Inc.) and an Andor Zyla 5.5 high-speed camera. The 3D-axis Helmholtz coils generate D.C. magnetic fields with a precision of 5% of the Earth's magnetic field (2.5 µT, manufacturer's specifications). The magnetic field was switched by applying -3.5 and +3.5 mT for the so-called U-turns, programmed at different time steps. The magnetic field values were fixed for 2 seconds before the switching value, and the switching was repeated over a fixed time-lapse, ensuring the observation of at least three U-turns in the field of view. The trajectories and U-turns were extracted and smoothed by a tracking script written in python and based on the OpenCV Object Tracking Algorithms with the CSRT tracker [27]. A convolution-based smoothing approach smooth the data. For the U-turn data, 12 cells from each condition were analyzed. A 40X objective (Nikon Apochromatic Lambda S 40X WI, N.A. 1.15, water immersion) was used for both trajectory and U-turn measurements. The mathematical relation to calculate the magnetic moment from the U-turn is the one used by C.J. Pierce et al. [28] valid for low field as those used in this study with the drag coefficient modification using the prolate ellipsoid approximation as done by P. Leao et al. considering length and width of the cels [30] :

$$\tau_{Uturn} = \frac{f_r}{M_{cell} \cdot H} = \frac{16 \cdot \pi \cdot \eta \cdot A^3}{3 \cdot M_{cell} \cdot H} \cdot$$

Here, $\boldsymbol{\tau_{Uturn}}$ corresponds to the time the MTB takes to make a U-turn upon switching the magnetic field (***H***); $\boldsymbol{\eta}$ corresponds to the media viscosity;M_{cell} to the magnetic moment of MSR-1 cell; ***A*** is defined as:

$$A = \frac{c^3}{\frac{1}{2}\left[\left(\frac{a+c}{a-c}\right) - \left(\frac{a \cdot c}{b^2}\right)\right]}$$

With a and b being the major and minor semi-axis respectively of the prolate ellipsoid and $c = \sqrt{(a^2 - b^2)}$;.The MSR-1 U-turn time ($\boldsymbol{\tau_{Uturn}}$) was determined by tracking the U-turn trajectory and then plotting its first derivate, corresponding to the instantaneous velocity. Note that the change in sign corresponds to the change in direction. The value of $\boldsymbol{\tau_{Uturn}}$ is obtained by taking the time

difference between the two steps as described in the section results and discussion, such that M_{cell} can then be calculated from equation (1).

M_{cell}. All data fitting was done by the intrinsic fitting functions of OriginPro[31] .

Fluorescent tagging efficiency

A semi-quantification analysis was done with a custom python script. The script extracts the fluorescence labeled MTB by converting the images to HSV and extracting the colored (fluorescent) layer to a new image and counting the amount of labeled MTB. The total amount (tagged and non-tagged) of MTB in the images are obtained by converting the image to gray scale and improving the image contrast with an adaptive histogram approach it then calculates the outline with a canny edge detector algorithm and finally the total outlines obtained were then counted. A relative error was then defined as total amount of MTB minus number of tagged MTB divided by the total amount of MTB and converted to percentage by multiplying by 100. This relative error was then considered as a parameter to compare the tagging efficiency.

Click chemistry

DBCO-PEG4-FLUOR 545 a.k.a. DBCO-PEG4-TAMRA (DBCO-TAMRA), was used to show the presence of the azide group after incorporating the modified amino acid. MSR-1 cells grown with the amino acid during 3 days (O.D (600 nm)= 0.2) were re-suspended in PBS (0.1 mM; pH 7.4) and mixed with 100 µM of DBCO-TAMRA for 1 hour while shaking at 700 rpm under dark conditions and at room temperature. The resulting solution was washed 3 times with PBS and centrifuged at 3500 g. For imaging, MSR-1 was left in PBS. For motility measurements, bacteria were re-suspended in FSM.

The attachment of the 10 µm, Micromer®-DBCO beads was done by adding 2 mg/mL of beads to a 2 mL solution of MTB (MTB-GFP) in PBS with an OD around 5.0 and left for 1 hour while shaking at 700 rpm under dark conditions and at room temperature. The resulting solution was washed 3 times with PBS and centrifuged at 3500 g. For imaging, MSR-1 was left in PBS. For motility measurements, they were re-suspended in FSM.

Results and Discussion

We used the strain MSR-1 as a model MTB, as this species is one of the most studied MTB. Figure 1 shows a fully grown MTB imaged with TEM with the typical black points indicating magnetosome particles (Figure 1A) as well as a growth curve (Figure 1B) and the semi-quantitative characterization of the magnetic properties by C_{mag}[32]. These C_{mag} values are obtained from the UV-VIS measurements and are directly proportional to cells' magnetization. C_{mag} is a relative value and depends on bacterial concentration and cellular length. To obtain a C_{mag} value from UV-VIS measurements, a spectrophotometer equipped with two sets of Helmotz coils, which are perpendicular one to another, is used. The Optical Density (OD) at 600 nm of a given bacterial suspension is first measured without applying any magnetic field. This measure is called ODx. Next, bacterial suspension's OD is measured when a magnetic field is applied in a y direction (ODy). Finally, bacterial suspension's OD is measured when a magnetic field is applied in a z direction (ODz) which is perpendicular to the y direction. C_{mag} is calculated using the following formula $\frac{ODy-ODz}{ODx}$.

Therefore, C_{mag} is an estimation of cellular magnetization (given that the difference ODy-ODz will depend on this parameter) normalized to cell density (ODx). From the growth curve, the generation or doubling time is calculated to be around 8 hours for different batches, in accordance with reported literature data [33,34]. It can be observed that after the complete formation of the magnetosomes, the C_{mag} stays constant. It is essential to highlight that when one needs to compare different batches with this method, special care has to be taken to cultures inoculation: the cultures have to be inoculated at low cellular density (e.g., [OD in the range of 0.009 - 0.02] in this case) to ensure enough bacterial divisions and therefore incorporation of the modified amino acid 3-azido-d-alanine hydrochloride in bacterial cell wall.. The typical MTB shapes observed from optical microscopy are presented in Figure 1 and are to be taken as a reference for the following analysis.

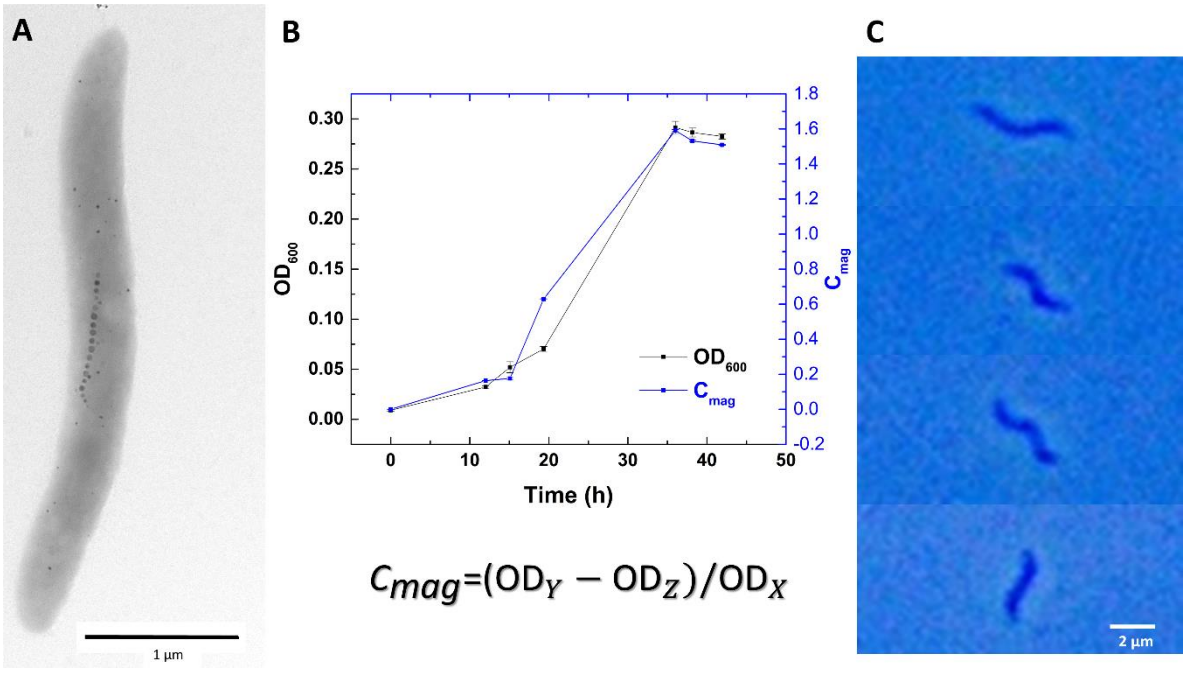

Figure 1: Basic physiological characterization of MSR-1 cells: A) TEM image of MSR-1 presenting the classical chain of magnetosomes. B) Combined plot presenting the average growth curve and cell magnetization (C_{mag}) obtained by UV-vis measurements for triplicate measurements of a cultured batch of MSR-1. The optical density (OD) was measured at 600 nm (ODx). OD,y,z are the optical densities in the presence of a y and z magnetic fields. C) Optical image displaying the MTB shapes observed to be used as reference.

We next moved to the first step of our process, corresponding to the incorporation of the azide groups. MSR-1 cells were grown in 3 different concentrations of the modified amino acid 3-Azido-D-alanine: 0.009 mM, 1.080 mM, and 1.800 mM. The TEM measurements together with the corresponding optical image for all three cases are shown in Figures 2A-2C. The TEM hints that the number of cells with magnetosome chains decreases upon increased modified amino acid and even more, the long cells do not show any magnetosome production. The growth curve shown at the top part of Figure 2D, indicates that for both 1.08 and 1.800 mM there is a clear delay in growth. The respective doubling times were calculated to be 6.69 ± 0.15 hours for 0.009 mM of azide, 7.048 ± 0.23 hours for 1.080 mM of azide and 9.08 ± 0.06 hours for 1.800 mM of azide. A non-parametrical statistical test was done (Kruskal-Wallis test) obtaining a p-value of 0.36 with alpha = 0.05 and

therefore the obtained doubling times cannot be considered significantly different. Analysis of C_{mag} evolution during growth showed that it decreases upon increasing modified amino acid concentration (Figure 2D). This decrease seems to be stronger during the exponential phase. To verify if this decrease in C_{mag} could be related to the cells being stressed upon the rise of modified amino acid concentration, the shape of the cells was analyzed by optical microscopy. Typical forms found for all 3 cases are presented beside the TEM images respectively, and cell shape changes are observed. For 1.080 mM many cells stop dividing and are much larger, indicating physiological stress. It is worth noticing that for all three cases, the cells were still motile, as observed from the videos in S1, S2, and S3.

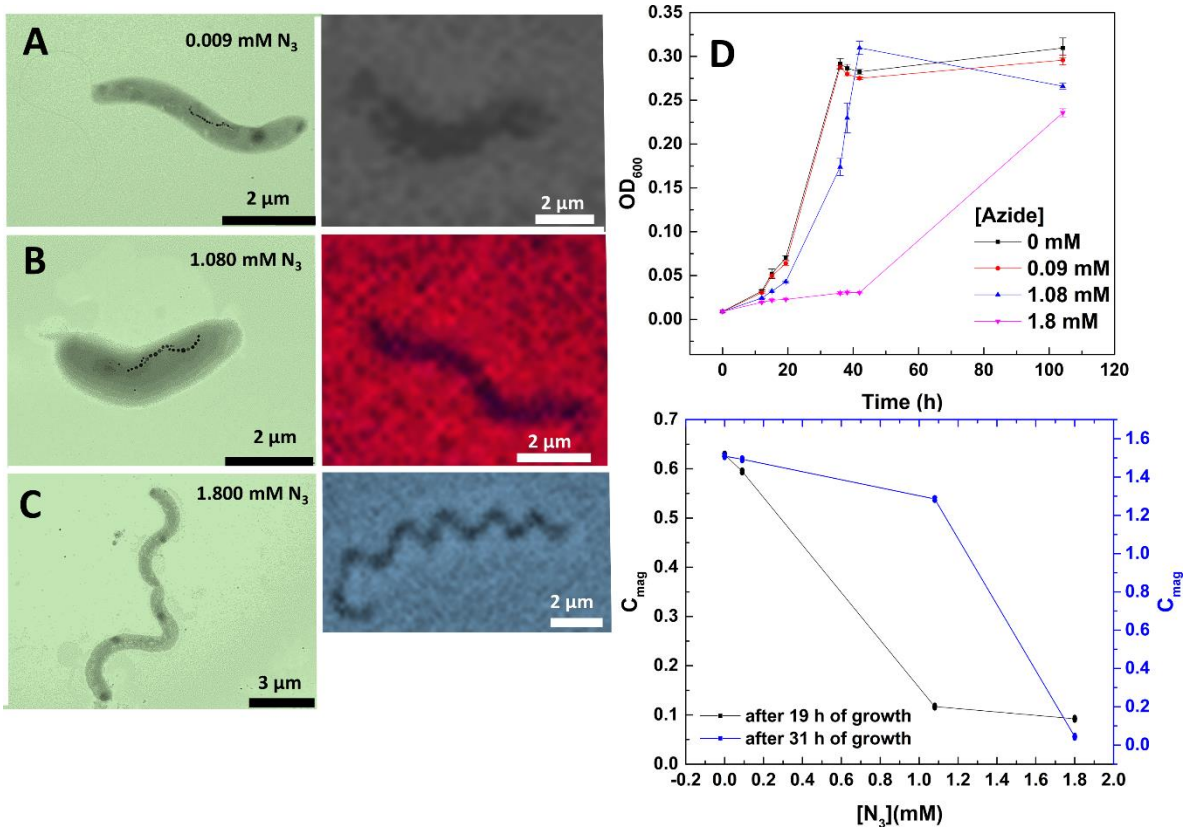

Figure 2: Characterization of the incorporation of the modified amino acid 3-azido-d-alanine hydrochloride in MSR-1. A) - E) show the TEM and optical images of MSR-1 grown in the presence of 0.009 mM, 1.080 mM and 1.800 mM modified amino acid. The plots in D, show the growth curve (top) for MSR-1 in the presence of the different concentrations of the modified amino acid and C_{mag} changes (bottom) for all concentrations after 19 and 31 hours of growth. All plots are the average of triplicate measurements and are plotted with the standard error as error bar.

We further performed U-turn analyses to assess cell magnetization quantitatively. For this analysis we exclude all long cells as no magnetosome were observed from the TEM measurements thus no response with external magnetic fields is expected. We therefore considered the average size found from 40 TEM images, namely length L= 3.46 ± 0.24 µm and width of W= 0.54±0.11 µm for the U-turn analysis. Briefly, the trajectory of a motile cell is recorded in the case in which an applied

magnetic field switches direction. This switching makes the cells do a U-turn and change direction. It is possible to calculate cell magnetization from the time it takes the cell to make the U-turn ([35] and method section). In Figure 3, cell magnetization and U-turn time for all 3 concentrations are shown, and the apparent decrease of cell magnetization upon modified amino acid concentration shown in Figure 2D is again observed. The same Figure is shown in Figure S1A together with the detailed graphs S1B-S1D necessary to calculate the U_{turn}. Figure S1B, shows a typical U-turn trajectory a single MSR-1 cell performs upon external magnetic field switching. Figure S1C shows the motion along a single direction (Y), displaying the change in orientation upon the applied magnetic field; the peak indicates this change in direction. Figure S1D shows the derivative of S1C and transforms the peak into a small step used to extract the U-turn time more precisely.

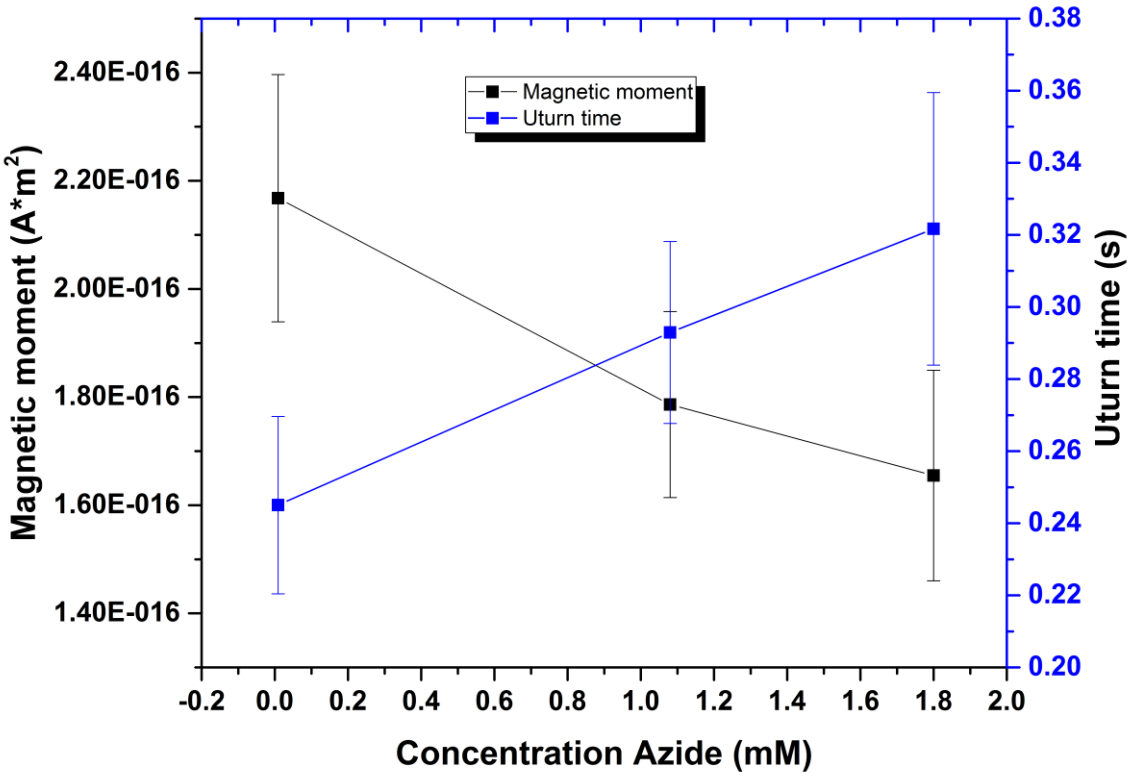

Figure 3: U-turn determination of *Cmag* for MSR-1. U-turn time and cell magnetization for MSR-1 grown in different concentrations of modified amino acid.

The presence of the biorthogonal azide group was verified, and for this, the batches grown with no modified amino acids, i.e., zero (control) and the same three concentrations, i.e. 0.009mM, 1.080 mM, and 1.800 mM of the modified amino acid were mixed with 100 µM of the fluorescent biomolecule DBCO-TAMRA. The samples were analyzed by confocal imaging, and the images are shown in Figures 4A-4D. The control shows some clusters of fluorescent biomolecules, but almost no MTB tagging (Figure 4A). The amount of MSR-1 tagged increases from 0.009 mM to 1.080 mM but decreases for 1.80 mM. A semi-quantification was done with a costum python script (see

method section). The script extracts the total amount of fluorescence labeled MTB and the total amount of MTB in the images. A relative error is then defined as total amount of MTB minus number of tagged MTB divided by the total amount of MTB and converted to percentage by multiplying by 100. This relative error is considered as a parameter to compare the tagging efficiency. Please note that this represents a minimum of tagging efficiency as it includes all MTB present in the images including those slightly out of focus that could potentially be tagged but not observed. We used 5 images for each azide concentration with over 100 MTB in each image and averaged the relative error. In table 1, the tagging efficiency for each used azide concentration is indicated.

Azide concentration (mM)	Tagging efficiency (%)
0.009	(5.30± 0.01)
1.080	(24.11± 0.02)
1.800	(17.57± 0.01)

Table1: Fluorescent tagging efficiency obtained for each azide concentration used.

The increased labeled number of MSR-1 cells observed for 1.080 mM suggests that this concentration is the best tested concentration (among those probed) allowing to have bacterial azide incorporation while retaining cell magnetization. Therefore, we considered this concentration and used it to exemplify the versatility of our approach with other tagging methods. Optical images with different functionalization are shown below: A single cell labeled with DAPI and TAMRA (Figure 4E and movie S3), TAMRA (Figure 4F), Cy5 (Figure 4G) and carboxyfluorescein (Figure 4H).

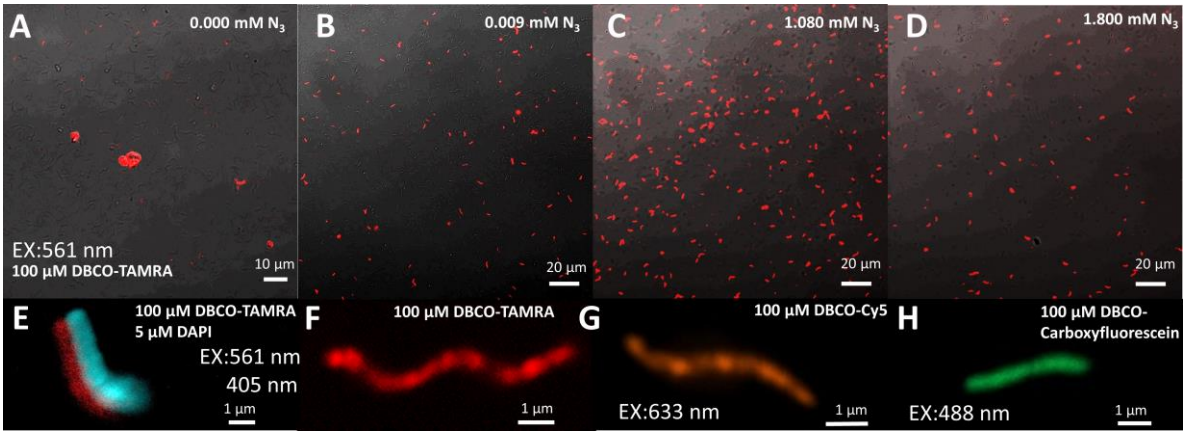

Figure 4: Fluorescent chemical compounds attachment by copper-free click-chemistry. A-D) 100 µM of DBCO-TAMRA attachment for MSR-1 grown in 4 different modified amino acid concentrations 0, 0.009, 1.080 and 1.800 mM, respectively. E) DNA staining by DAPI in conjunction with DBCO-TAMRA with double excitation source 405 nm for DAPI and 561 nm for TAMRA. F-H) A single-cell image for MSR-1 with DBCO-PEG4-FLUOR 545; DBCO-Cy5 and DBCO-dPEG ®12-carboxyfluorescein.

We analyzed the attachment to relatively large, 10 µm, Micromer®-DBCO beads. In figure 5 A) an optical image is presented showing the effective attachment of N_3 modified MSR-1 to the Micromer®-DBCO beads in different configurations and in B) the N_3 modified MSR-1 are shown to attach homogenously over the surface. Figure 5 C) shows a combined optical and fluorescence

image of the same Micromer®-DBCO beads in the presence of N_3 modified GFP tagged MSR-1, The blurred background are swimming MSR-1. Figure 5 D) shows the GFP fluorescence solely demonstrating the attachment on the beads surface. We checked if the beads with attached bacteria presented any motion or magnetic response and verified that there was none. Movie S5 indicates that the beads with the attached MSR-1 do not present any directional motion while movie S6 shows that even with high number of attached MSR-1 there still is no motion. In Movie 7 we used a custom magnetic microscope [26] to apply a 3mT rotating magnetic field and show the lack of response form the bead together with the rotating MSR-1.

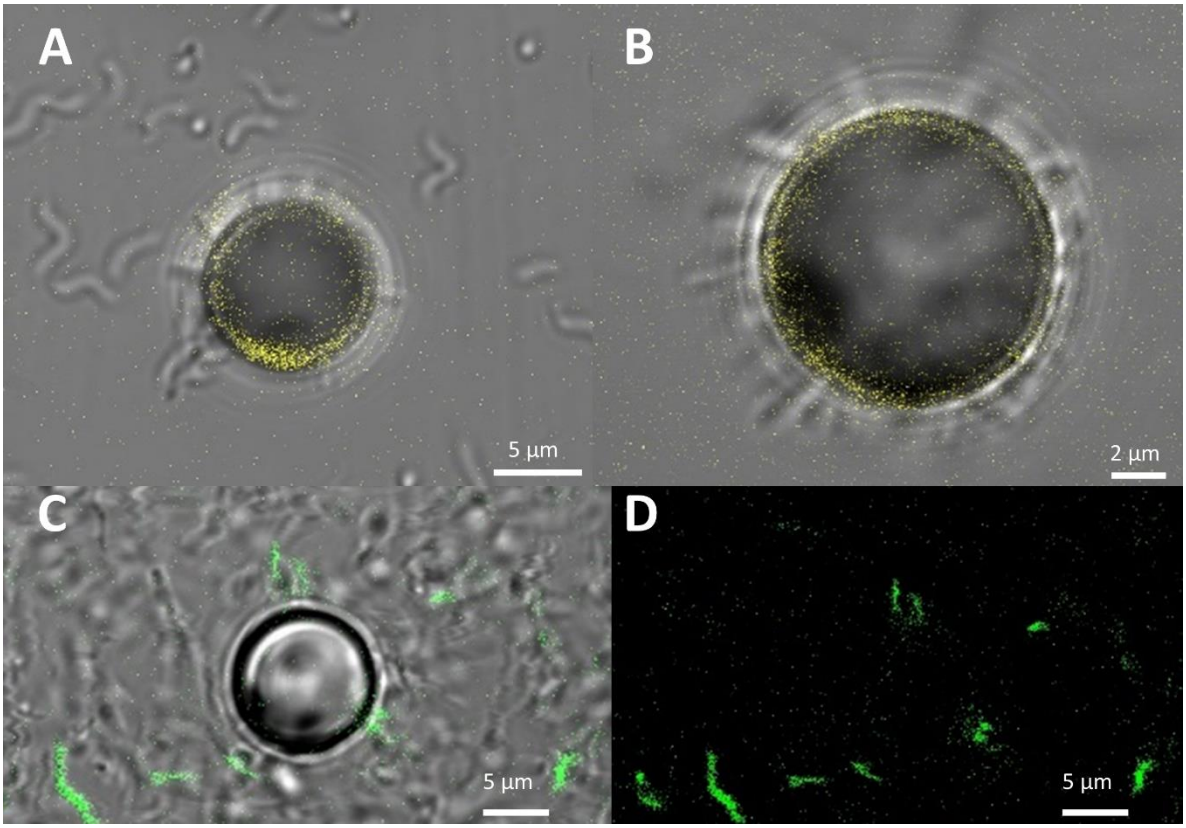

Figure 5: A) and B) show the optical image of the 10µm Micromer® beads with N_3 modified MSR-1 attached to the surface. The Micromer® beads show fluorescence at n excitation wavelength of 405 nm. Similarly C) shows combined fluorescence (excitation wavelength of 488 nm) and bright field MSR1-GGFP-N_3 attached to the beads and D) only the GFP Fluorescence from MSR-1.

Compared with previous works, while assuming that the available surface of the bacteria is the same between each culture batch of a given strain, the immobilization success rate depends on two things: 1) the yield of bonding and 2) the yield of healthy bacteria. The click chemistry is bio-orthogonal and compatible with different biomolecules. Nevertheless, as shown here, the azide group incorporation through metabolic labeling can influence the physiological properties of MTB, specifically magnetosome production. It remains to be seen if a similar effect occurs when bacteria are genetically engineered. For example, overproduction of magnetosomes has been observed previously by genomic amplification [36].

For nanoparticles, several studies have shown a higher immobilization yield through click chemistry compared to carbodiimide (EDC/NHS chemistry) [37,38]. Carbodiimide was previously used to attach nanoliposomes on MTB (specifically to the strain *Manetococcus marinus* (MC-1) [9]). The chemical conjugation of liposomes functionalized with reactive groups (–COOH) allows the covalent binding to primary amino groups ($–NH_2$) intrinsic to bacterial cell membrane proteins. Another approach that bonds cargo to the primary groups of a MTB, more specifically to *Magnetospirilium magneticum* (AMB-1), was presented [11]. The authors used an MTB/PEG–biotin complex, corresponding to a covalent bond formation between bacteria and biotin–PEG–NHS polymer. In that case, the main mechanism also includes a nucleophilic attack as in the case of EDC/NHS where NHS esters are formed and attached to the primary amino groups leaving the biotin-PEG-NHS on the bacteria surface and allowing further functionalization by streptavidin-biotin interaction. A third approach introduced immobilized Indocyanine green nanoparticles (INPs) functionalized with maleimide groups on AMB-1 [10]. The INPs were chemically conjugated to activated sulfhydryl on the surface of AMB-1 bacteria by Michael addition reaction. Overall, just looking at an individual cell, the amount of cargo that can be immobilized will then depend on the available functional groups, amino, activated sulfhydryl (activated disulfide surface proteins) or in our case the amount of azide groups and of course the affinity and selectivity of the bonding at hand. Click chemistry has the advantage of selectivity and therefore of yield when compared to the other immobilization techniques. Another advantage of the present work is that we do not need to activate surface groups. Still in all cases, many steps are needed to add or have available chemical groups and attach the cargo. The click chemistry has the advantage, compared to other covalent immobilization techniques used, of the bio-orthogonality and selectivity of the reactions. However, it still presents the disadvantage that to achieve the immobilization of specific groups on the biomolecule and bacterial surface, several reaction steps must be carried out on the respective units to prepare them for the click reaction. The problem of having several reaction steps could be partially overcome by, for example, bacterial genetic engineering. Nevertheless, as demonstrated in this work, care must be taken to find the right conditions to maintain the MTB's general physiological properties. In this work we also show the effective attachment to 10 µm Micromer®-DBCO beads. However, this attachment prevents bacterial motion and magnetic response. We attribute this lack of response to the size of the beads as they precipitate and get fixed to the glass slide adding additional resistance to external forces. We envision that smaller particles should allow directional motion stirred by the MTB as shown in previous work [9].

The copper-free strain-promoted azide-alkyne cycloaddition is one of the most widely employed in bio-orthogonal chemistry and, as indicated previously, has been employed by other bacteria to attach cargo [25]. However, in the mentioned work, the physiological properties of the bacterium *E. coli strain Seattle 1946* used were not studied. The binding efficiency was assessed on fixed bacteria, and the motility after modification was assumed to have negligible changes compared to the non-modified bacteria referring to a previous work that indicated a 65 % decrease in speed at the highest bacteria motility of a bacterium with cargo compared to a free bacterium [39]. It was not experimentally tested, nor was the shape of the bacterium analyzed upon different azide concentrations to see if any physiological stress builds up. Although in our work, we also do not observe a clear change in speed, the MTB growth is clearly affected showing difference in shape and even effects upon the biosynthesis of magnetosomes. Fixating bacteria and inhibiting their growth are most likely the reasons, as the physiological stress build-up was not observed previously.

Conclusion

Copper-free click chemistry was successfully proven by mixing DBCO- TAMRA with MTB where a modified amino acid was integrated into the periplasm. The best conditions for the azide incorporation were then used to show its compatibility with other tagging methods such as DAPI and biomolecules by single cell confocal imaging. In addition, we exemplarily have attached 10 µm DBCO-Polystyrene beads. However, due to their dimension, the beads sediment to the glass and get fixed. Despite the fixation, many MTB are capable of attaching to the beads using the protocol we have developed. We observe that to maintain bacterial mobility once attached, smaller particles should be used. These findings open the possibilities of designing MTB functionalized through click chemistry with any biomolecules and are extremely important for future MTB bots designs or MTB applied to bio-sensing, energy or environmental applications where functionalized MTB are envisioned for increased performance [40].

Acknowledgement

The project leading to this publication has received funding from the Excellence Initiative of Aix-Marseille Univeristy – A*Midex, a French “Investissements d’Avenir” programme.

Supporting information

Movie S1 shows motile MSR-1 grown with 0.005 mM of modified amino azide with a +/-3.5mT magnetic field applied along the vertical, y, direction, switching every 2 sec once the field is activated.

Movie S2 shows motile MSR-1 grown with 0.06 mM of modified amino azide with a +/-3.5mT magnetic field applied along the vertical, y, direction, switching every 2 sec once the field is activated.

Movie S3 shows motile MSR-1 grown with 0.1 mM of modified amino azide with a +/-3.5mT magnetic field applied along the vertical, y, direction, switching every 2 sec once the field is activated.

Movie S4 shows overlaying optical and confocal imaging of the tagged MTB with DAPI and TAMRA.

Movie S5 shows 10µm Micromer® beads with N_3 modified MSR-1 attached to the surface with different configuration

Movie S6 shows 10µm Micromer® beads with N_3 modified MSR-1 homogenously attached to the surface

Movie S7 shows 10µm Micromer® beads with N_3 modified MSR-1 attached to the surface with an 3mT rotating magnetic field.

Figure S1 presents the graphs showing related to the Uturn measurement and cell magnetization determination.

References

[1] F. Soto, R. Chrostowski, Frontiers of Medical Micro/Nanorobotics: in vivo Applications and Commercialization Perspectives Toward Clinical Uses, Front. Bioeng. Biotechnol. 6 (2018) 170. https://doi.org/10.3389/fbioe.2018.00170.

[2] H. Zhou, C.C. Mayorga-Martinez, S. Pané, L. Zhang, M. Pumera, Magnetically Driven Micro and Nanorobots, Chem. Rev. 121 (2021) 4999–5041. https://doi.org/10.1021/acs.chemrev.0c01234.

[3] A. Coene, J. Leliaert, Magnetic nanoparticles in theranostic applications, J. of Appl. Phys. 131 (2022) 160902. https://doi.org/10.1063/5.0085202.

[4] S. Martel, Swimming microorganisms acting as nanorobots versus artificial nanorobotic agents: A perspective view from an historical retrospective on the future of medical nanorobotics in the largest known three-dimensional biomicrofluidic networks, Biomicrofluidics. 10 (2016) 021301. https://doi.org/10.1063/1.4945734.

[5] A. Sahari, M.A. Traore, A.M. Stevens, B.E. Scharf, B. Behkam, Toward Development of an Autonomous Network of Bacteria-Based Delivery Systems (BacteriaBots): Spatiotemporally High-Throughput Characterization of Bacterial Quorum-Sensing Response, Anal. Chem. 86 (2014) 11489–11493. https://doi.org/10.1021/ac5021003.

[6] B. Mostaghaci, O. Yasa, J. Zhuang, M. Sitti, Bioadhesive Bacterial Microswimmers for Targeted Drug Delivery in the Urinary and Gastrointestinal Tracts, Adv. Sci. 4 (2017) 1700058. https://doi.org/10.1002/advs.201700058.

[7] O. Schauer, B. Mostaghaci, R. Colin, D. Hürtgen, D. Kraus, M. Sitti, V. Sourjik, Motility and chemotaxis of bacteria-driven microswimmers fabricated using antigen 43-mediated biotin display, Sci Rep. 8 (2018) 9801. https://doi.org/10.1038/s41598-018-28102-9.

[8] J. Bastos-Arrieta, A. Revilla-Guarinos, W.E. Uspal, J. Simmchen, Bacterial Biohybrid Microswimmers, Front. Robot. AI. 5 (2018) 97. https://doi.org/10.3389/frobt.2018.00097.

[9] O. Felfoul, M. Mohammadi, S. Taherkhani, D. de Lanauze, Y. Zhong Xu, D. Loghin, S. Essa, S. Jancik, D. Houle, M. Lafleur, L. Gaboury, M. Tabrizian, N. Kaou, M. Atkin, T. Vuong, G. Batist, N. Beauchemin, D. Radzioch, S. Martel, Magneto-aerotactic bacteria deliver drug-containing nanoliposomes to tumour hypoxic regions, Nat. Nanotechnol. 11 (2016) 941–947. https://doi.org/10.1038/nnano.2016.137.

[10] J. Xing, T. Yin, S. Li, T. Xu, A. Ma, Z. Chen, Y. Luo, Z. Lai, Y. Lv, H. Pan, R. Liang, X. Wu, M. Zheng, L. Cai, Sequential Magneto-Actuated and Optics-Triggered Biomicrorobots for Targeted Cancer Therapy, Adv. Funct. Mater. (2020) 2008262. https://doi.org/10.1002/adfm.202008262.

[11] R. Chaturvedi, Y. Kang, Y. Eom, S.R. Torati, C. Kim, Functionalization of Biotinylated Polyethylene Glycol on Live Magnetotactic Bacteria Carriers for Improved Stealth Properties, Biology. 10 (2021) 993. https://doi.org/10.3390/biology10100993.

[12] C.T. Lefevre, D.A. Bazylinski, Ecology, Diversity, and Evolution of Magnetotactic Bacteria, Microbiol. Mol. Bio. Rev. 77 (2013) 497–526. https://doi.org/10.1128/MMBR.00021-13.

[13] C.T. Lefèvre, M. Bennet, L. Landau, P. Vach, D. Pignol, D.A. Bazylinski, R.B. Frankel, S. Klumpp, D. Faivre, Diversity of Magneto-Aerotactic Behaviors and Oxygen Sensing Mechanisms in Cultured Magnetotactic Bacteria, Biophys. J. 107 (2014) 527–538. https://doi.org/10.1016/j.bpj.2014.05.043.

[14] D. Kuzajewska, A. Wszołek, W. Żwierełło, L. Kirczuk, A. Maruszewska, Magnetotactic Bacteria and Magnetosomes as Smart Drug Delivery Systems: A New Weapon on the Battlefield with Cancer?, Biology. 9 (2020) 102. https://doi.org/10.3390/biology9050102.

[15] S. Mériaux, M. Boucher, B. Marty, Y. Lalatonne, S. Prévéral, L. Motte, C.T. Lefèvre, F. Geffroy, F. Lethimonnier, M. Péan, D. Garcia, G. Adryanczyk-Perrier, D. Pignol, N. Ginet, Magnetosomes, Biogenic Magnetic Nanomaterials for Brain Molecular Imaging with 17.2 T MRI Scanner, Adv. Healthcare Mater. 4 (2015) 1076–1083. https://doi.org/10.1002/adhm.201400756.
[16] A. Kraupner, D. Eberbeck, D. Heinke, R. Uebe, D. Schüler, A. Briel, Bacterial magnetosomes – nature's powerful contribution to MPI tracer research, Nanoscale. 9 (2017) 5788–5793. https://doi.org/10.1039/C7NR01530E.
[17] A.V. Makela, M.A. Schott, C.S. Madsen, E.M. Greeson, C.H. Contag, Magnetic Particle Imaging of Magnetotactic Bacteria as Living Contrast Agents Is Improved by Altering Magnetosome Arrangement, Nano Lett. 22 (2022) 4630–4639. https://doi.org/10.1021/acs.nanolett.1c05042.
[18] N.K. Devaraj, M.G. Finn, Introduction: Click Chemistry, Chem. Rev. 121 (2021) 6697–6698. https://doi.org/10.1021/acs.chemrev.1c00469.
[19] B.T. Worrell, J.A. Malik, V.V. Fokin, Direct Evidence of a Dinuclear Copper Intermediate in Cu(I)-Catalyzed Azide-Alkyne Cycloadditions, Science. 340 (2013) 457–460. https://doi.org/10.1126/science.1229506.
[20] L. Li, Z. Zhang, Development and Applications of the Copper-Catalyzed Azide-Alkyne Cycloaddition (CuAAC) as a Bioorthogonal Reaction, Molecules. 21 (2016) 1393. https://doi.org/10.3390/molecules21101393.
[21] J.W. Chin, S.W. Santoro, A.B. Martin, D.S. King, L. Wang, P.G. Schultz, Addition of *p* -Azido- L - phenylalanine to the Genetic Code of *Escherichia c oli*, J. Am. Chem. Soc. 124 (2002) 9026–9027. https://doi.org/10.1021/ja027007w.
[22] S. Reddington, P. Watson, P. Rizkallah, E. Tippmann, D.D. Jones, Genetically encoding phenyl azide chemistry: new uses and ideas for classical biochemistry, Biochem. Soc. Trans. 41 (2013) 1177–1182. https://doi.org/10.1042/BST20130094.
[23] P.V. Chang, J.A. Prescher, E.M. Sletten, J.M. Baskin, I.A. Miller, N.J. Agard, A. Lo, C.R. Bertozzi, Copper-free click chemistry in living animals, Proc. Natl. Acad. Sci. U.S.A. 107 (2010) 1821–1826. https://doi.org/10.1073/pnas.0911116107.
[24] V.M. Moreno, E. Álvarez, I. Izquierdo-Barba, A. Baeza, J. Serrano-López, M. Vallet-Regí, Bacteria as Nanoparticles Carrier for Enhancing Penetration in a Tumoral Matrix Model, Adv. Mater. Interfaces. 7 (2020) 1901942. https://doi.org/10.1002/admi.201901942.
[25] U. Heyen, D. Schüler, Growth and magnetosome formation by microaerophilic Magnetospirillum strains in an oxygen-controlled fermentor, Appl Microbiol Biotechnol. 61 (2003) 536–544. https://doi.org/10.1007/s00253-002-1219-x.
[26] M. Bennet, A. McCarthy, D. Fix, M.R. Edwards, F. Repp, P. Vach, J.W.C. Dunlop, M. Sitti, G.S. Buller, S. Klumpp, D. Faivre, Influence of Magnetic Fields on Magneto-Aerotaxis, PLoS ONE. 9 (2014) e101150. https://doi.org/10.1371/journal.pone.0101150.
[27] N. Dardagan, A. Brdanin, D. Dzigal, A. Akagic, Multiple Object Trackers in OpenCV: A Benchmark, in: 2021 IEEE 30th International Symposium on Industrial Electronics (ISIE), IEEE, Kyoto, Japan, 2021: pp. 1–6. https://doi.org/10.1109/ISIE45552.2021.9576367.
[28] C.J. Pierce, E. Mumper, E.E. Brown, J.T. Brangham, B.H. Lower, S.K. Lower, F.Y. Yang, R. Sooryakumar, Tuning bacterial hydrodynamics with magnetic fields, Phys. Rev. E. 95 (2017) 062612. https://doi.org/10.1103/PhysRevE.95.062612.
[29] M.P. Pichel, T.A.G. Hageman, I.S.M. Khalil, A. Manz, L. Abelmann, Magnetic response of Magnetospirillum gryphiswaldense observed inside a microfluidic channel, Journal of Magnetism and Magnetic Materials. 460 (2018) 340–353. https://doi.org/10.1016/j.jmmm.2018.04.004.

[30] P. Leão, L. Le Nagard, H. Yuan, J. Cypriano, I. Da Silva-Neto, D.A. Bazylinski, D. Acosta-Avalos, H.L. Barros, A.P. Hitchcock, U. Lins, F. Abreu, Magnetosome magnetite biomineralization in a flagellated protist: evidence for an early evolutionary origin for magnetoreception in eukaryotes, Environ Microbiol. 22 (2020) 1495–1506. https://doi.org/10.1111/1462-2920.14711.
[31] OriginPro, Originlab Corporation, Northhampton, MA, USA, (2016).
[32] D. Schüler, R. Uhl, E. Bäuerlein, A simple light scattering method to assay magnetism in *Magnetospirillum gryphiswaldense*, FEMS Microbiology Letters. 132 (1995) 139–145. https://doi.org/10.1111/j.1574-6968.1995.tb07823.x.
[33] C.N. Riese, R. Uebe, S. Rosenfeldt, A.S. Schenk, V. Jérôme, R. Freitag, D. Schüler, An automated oxystat fermentation regime for microoxic cultivation of Magnetospirillum gryphiswaldense, Microb Cell Fact. 19 (2020) 206. https://doi.org/10.1186/s12934-020-01469-z.
[34] I. Kolinko, C. Jogler, E. Katzmann, D. Schüler, Frequent Mutations within the Genomic Magnetosome Island of Magnetospirillum gryphiswaldense Are Mediated by RecA, J Bacteriol. 193 (2011) 5328–5334. https://doi.org/10.1128/JB.05491-11.
[35] D.M.S. Esquivel, H.G. de P.L. de. Barros, Motion of magnetotactic microorganisms, Brazil, 1985. http://inis.iaea.org/search/search.aspx?orig_q=RN:17012441.
[36] A. Lohße, I. Kolinko, O. Raschdorf, R. Uebe, S. Borg, A. Brachmann, J.M. Plitzko, R. Müller, Y. Zhang, D. Schüler, Overproduction of Magnetosomes by Genomic Amplification of Biosynthesis-Related Gene Clusters in a Magnetotactic Bacterium, Appl. Environ. Microbiol. 82 (2016) 3032–3041. https://doi.org/10.1128/AEM.03860-15.
[37] D.L.J. Thorek, ew R. Elias, A. Tsourkas, Comparative Analysis of Nanoparticle-Antibody Conjugations: Carbodiimide Versus Click Chemistry, Mol Imaging. 8 (2009) 7290.2009.00021. https://doi.org/10.2310/7290.2009.00021.
[38] J. Bolley, E. Guenin, N. Lievre, M. Lecouvey, M. Soussan, Y. Lalatonne, L. Motte, Carbodiimide versus Click Chemistry for Nanoparticle Surface Functionalization: A Comparative Study for the Elaboration of Multimodal Superparamagnetic Nanoparticles Targeting $\alpha_v\beta_3$ Integrins, Langmuir. 29 (2013) 14639–14647. https://doi.org/10.1021/la403245h.
[39] M.A. Traore, C.M. Damico, B. Behkam, Biomanufacturing and self-propulsion dynamics of nanoscale bacteria-enabled autonomous delivery systems, Appl. Phys. Lett. 105 (2014) 173702. https://doi.org/10.1063/1.4900641.
[40] N. Ebrahimi, C. Bi, D.J. Cappelleri, G. Ciuti, A.T. Conn, D. Faivre, N. Habibi, A. Hošovský, V. Iacovacci, I.S.M. Khalil, V. Magdanz, S. Misra, C. Pawashe, R. Rashidifar, P.E.D. Soto-Rodriguez, Z. Fekete, A. Jafari, Magnetic Actuation Methods in Bio/Soft Robotics, Adv. Funct. Mater. 31 (2021) 2005137. https://doi.org/10.1002/adfm.202005137.